Polyhedron 208 (2021) 115389

Contents lists available at ScienceDirect

Polyhedron

journal homepage: www.elsevier.com/locate/poly

A high-frequency EPR study of magnetic anisotropy and intermolecular interactions of Co(II) ions

Lena Spillecke [a,*], Shalini Tripathi [c], Changhyun Koo [a], Mursaleem Ansari [c], Shefali Vaidya [c], Amaleswari Rasamsetty [c], Talal Mallah [d], Gopalan Rajaraman [c], Maheswaran Shanmugam [c,*], Rüdiger Klingeler [a,b,*]

[a] Kirchhoff Institute for Physics, Heidelberg University, 69120 Heidelberg, Germany
[b] Centre for Advanced Materials, Heidelberg University, 69120 Heidelberg, Germany
[c] Department of Chemistry, Indian Institute of Technology Bombay, Powai, Mumbai 400076, Maharashtra, India
[d] Institut de Chimie Moléculaire et des Matériaux d'Orsay, CNRS, Université Paris Sud, Université Paris Saclay, 15, rue Georges Clemenceau, 91405 Orsay Cedex, France

ARTICLE INFO

Keywords:
HF-EPR
Cobalt
Exchange interaction
Second coordination sphere
SMM

ABSTRACT

Changing the anion in a crystal lattice induces distinct structural distortions in the $[CoS_4]^{2+}$ core for a family of complexes with the general molecular formula $[Co(L_1)_4]X_2$, where L_1 = thiourea (NH_2CSNH_2) and X = I (**1**), Br (**2**), and $[Co(L_1)_4](SiF_6)$ (**3**). The magnetic anisotropy (D) for **1**–**3** was quantitatively determined with a magnitude of −153(2), −168(5) and < -400 GHz, respectively, by HF-EPR investigation. Also, intermolecular exchange interactions were determined experimentally, whereby an antiferromagnetic exchange for **1** (-5.5 GHz) and **2** (-4.1 GHz), and a ferromagnetic interaction for **3** (+3.5 GHz) are witnessed (based on $H = -JS_1S_2$). The exchange interactions, computed using DFT methods on a model complex of **1**, disclose the presence of an antiferromagnetic exchange interaction, consistent with the experimental observation. Overall, the present study provides convincing experimental evidence for the sizable influence not only of the first but also of the second coordination sphere on the magnetic anisotropy and exchange interactions of Co(II) ions.

1. Introduction

Tuning magnetic anisotropy and ligand fields of metal–organic complexes, and thereby controlling the slow-relaxation behaviour in single-molecule magnets (SMMs), is a key prerequisite to exploit these materials as a future alternative to conventional data storages [1–3]. As an alternative to multi-centre SMMs, which offer the potential of very large spin quantum numbers with however often reduced magnetic anisotropy, restricting to systems with only a single paramagnetic centre, i.e. so-called single-ion magnets (SIM), offers a route to more simple model systems with significant anisotropy [4–11]. Due to large unquenched magnetic moments and large intrinsic magnetic anisotropy, many lanthanide-based SIMs have been investigated which offer record values for magnetic anisotropy barriers [12–15]. Transition metal ions with (partly) unquenched orbital moments provide another promising route towards novel SIMs [16–18].

Distorted tetrahedrally-coordinated high-spin Co(II) monomers exhibit relatively strong spin–orbit coupling and their electronic properties can be tuned by variation of the crystal field [19–24]. The half-integer magnetic ground state of high-spin Co(II) ions prevents quantum tunnelling mechanisms [25], thus allowing the observation of slow relaxation of the magnetisation in the absence of external magnetic fields [6,9,26–29]. Tuning of the spin Hamiltonian parameters is typically achieved by variation of the first coordination sphere around the central ion [29–33]. However, as reported recently, the second or peripheral coordination spheres can also have a significant impact, not only on the magnitude but also on the nature (e.g. the sign of the axial anisotropy parameter *D*) of the magnetic anisotropy [28,34–40]. In order to quantitatively investigate these effects and to understand the electronic structure of Co(II)-complexes and the magnetic relaxation mechanisms, precise determination of the spin Hamiltonian (SH) parameters (*g*-value, axial and transversal anisotropy parameters *D* and *E*)

* Corresponding authors at: Kirchhoff Institute for Physics, Heidelberg University, 69120 Heidelberg and Department of Chemistry, Indian Institute of Technology Bombay, Powai, Mumbai 400076, Maharashtra, India.
E-mail addresses: lena.spillecke@kip.uni-heidelberg.de (L. Spillecke), eswar@chem.iitb.ac.in (M. Shanmugam), ruediger.klingeler@kip.uni-heidelberg.de (R. Klingeler).

https://doi.org/10.1016/j.poly.2021.115389
Received 10 May 2021; Accepted 15 July 2021
Available online 26 July 2021

are mandatory. The zero-field splitting (ZFS) induced by the axial single-ion magnetic anisotropy (associated with the parameter D) for Co(II)-containing systems is, however, often too large to be measured by conventional electron paramagnetic resonance (EPR) techniques since both the X- and Q-bands cannot be employed as $D \gg h\nu$ implies the absence of allowed EPR signals at the frequencies ν. To investigate such systems, high-frequency/high field electron paramagnetic resonance (HF-EPR) measurements are usually used [41,42]. In this article we present detailed tuneable HF-EPR studies on three high-spin Co(II)-monomers, namely $[Co(L_1)_4]I_2$ (**1**), $[Co(L_1)_4]Br_2$ (**2**) and $[Co(L_1)_4]SiF_6$ (**3**), where L_1 = thiourea (NH_2CSNH_2).

The influence of the secondary coordination on the modulation of the magnetic anisotropy of Co(II) ions is known theoretically [27,28,35,37,38], but experimental evidence, measured on the significant influence which was found for other complexes, is currently relatively scarce in the literature [29,37,38,43,44]. The present work furnishes a further experimental proof for the impact of the variation of the secondary coordination sphere on the magnetic anisotropy of Co(II) ions. The theoretical calculations are in excellent agreement with the experimental observations (*vide infra*) [37].

Besides a detailed investigation on the single ion behaviour of the Co (II) centres, we also observed small intermolecular super-exchange interactions in the range of a few GHz (~3–6 GHz) for all three complexes, which are beyond the resolvable energy scale of a standard SQUID magnetometer. Quantification of these interactions reveals that not only the strength but also the sign changes based on the anions in the crystal lattice, which have an influence on the secondary coordination sphere. Finite intermolecular interactions can play a crucial role in the suppression of slow magnetic relaxation behaviour in such complexes [45–48], therefore, this investigation can help to tune single ion properties via controlling supramolecular interactions by changing the cations/anions in the crystal lattice. This mechanism is discussed in detail in the present study.

2. Experimental section

The complexes investigated in this article were synthesised as reported by us earlier [37]. High-frequency/high-field electron paramagnetic resonance (HF-EPR) measurements were performed using a millimeter vector network analyser (MVNA) from ABmm as a phase sensitive microwave source and detector [49]. The spectra were obtained in the frequency range 70–600 GHz and in external magnetic fields of up to 16 T. Temperature control between 2 and 80 K was ensured by a variable temperature insert (VTI) with a He gas flow. The powder samples were placed inside a brass ring in the form of a loose powder, i.e. no extra glue or grease was used. This setup enables alignment of the crystallites in the external magnetic fields, which was performed by means of applying the maximum field of 16 T prior to the measurements. During this initial field sweep, alignment was ensured by monitoring the corresponding alignment jumps in the transmitted microwave signal. In addition, rearrangement of the crystallites was avoided by restricting the magnetic field to the range 0.2 to 16 T. Analysis of the data was done using the EasySpin software package [50].

Broken Symmetry Density Functional Theory (BS-DFT) calculations were performed on the full coordinates of the crystallographic structure of **1** using unrestricted hybrid B3LYP functionals [51], with the all electron Alhrich's triple-ζ valence (TZV) [52,53] basis set for all the elements, as implemented in the Gaussian 09 suite of programs [54]. The magnetic exchange coupling interaction was calculated on binuclear models that were generated from the crystal structure of **1** and the exchange coupling between the two high spin monomeric Co(II) ions was described by the Heisenberg-Dirac-van Vleck (HDVV) Hamiltonian as follows:

$$H_{HDVV} = -JS_1S_2 \quad (1)$$

This Hamiltonian was used to describe the intermolecular interactions throughout the manuscript in all sections.

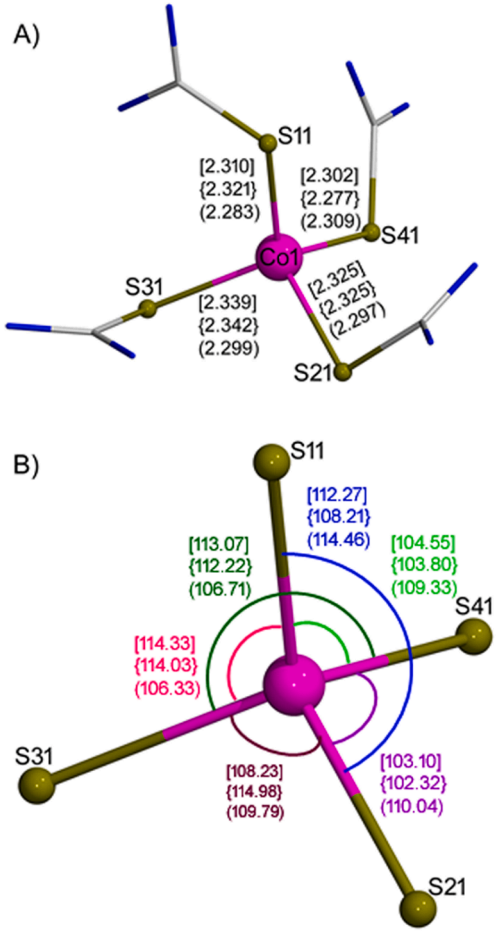

Fig. 1. Representative molecular structure of complex **1**. Hydrogen atoms are removed for clarity. Colour code: grey = C and blue = N. The parameters in the square, curly and round brackets correspond to the bond lengths (Å, panel A) and bond angles (°, panel B) for **1**, **2** and **3**, respectively. ((Colour online.))

For the estimation of the magnetic coupling, Hartree–Fock or DFT methods, together with the broken symmetry (BS) model developed by Noodleman and co-workers, have been employed, coupled with the equation proposed by Ruiz and co-workers.[55–57]

$$J = \frac{(E_{BS} - E_{HS})}{2S_1S_2 + S_2} \quad (2)$$

3. Results and discussion

By employing the thiourea ligand with the corresponding cobalt precursors, we have isolated three different cobalt monomeric complexes (**1**–**3**). The detailed synthesis, as well as the structural description, along with the crystallographic parameters of all the complexes, were recently reported by us [37].

Complexes **1**–**3** are structurally analogous to each other. The four coordination sites of the Co(II) ions in the complexes are occupied by sulfur ligands. Thus, the Co(II) ions exhibit a distorted tetrahedral geometry. The overall cationic charge in the coordination sphere of **1**–**3** is satisfied by two iodides, two bromides and one SiF_6 anion in the crystal lattice, respectively. A representative molecular structure of **1** is shown in Fig. 1. Selected bond lengths and bond angles for the structurally analogous complexes of **1**–**3** are provided in Fig. 1(A) and (B), respectively.

To understand the geometry around the Co(II) ion, we have performed continuous shape measurement (CShM) analysis, which

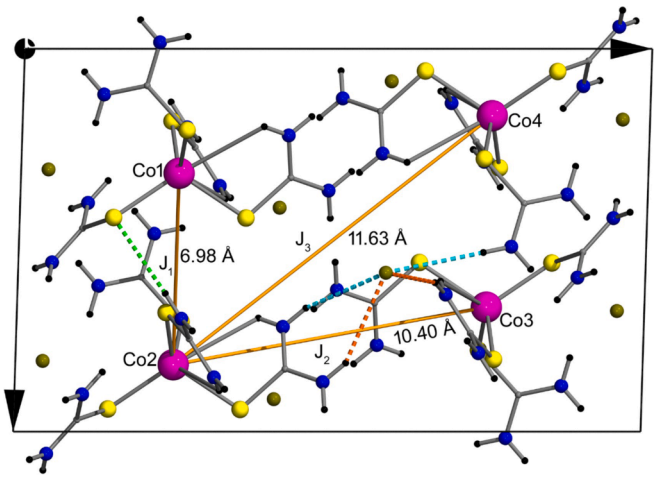

Fig. 2. The packing diagram of **1** (view along the b-axis) shows the interatomic distance between the molecules in the crystal lattice. The dotted bonds represent the intermolecular H-bonding between the molecules in the crystal lattice.

indicates that all three complexes display a distorted tetrahedral geometry (Table S1). For the molecules **1**–**3** the CShM values are estimated to be 0.28, 0.22 and 0.09, respectively, with respect to the ideal T_d geometry. The obtained values suggest, that complex **1** has a higher distortion with respect to the ideal tetrahedral geometry around the Co (II) ion compared to the complexes **2** and **3**. This can be attributed to the change of the anion in the crystal lattice for complexes **1**–**3**. Further, we would like to emphasize that depending on the identity and orientation of the anions in the crystal lattice of these complexes, a distinct supramolecular interaction, namely H-bonding, is observed. Furthermore, the strength of H-bonding differs for all the observed complexes, e.g. the H-bonding strength in **1** is stronger than that in **2**. Consequently, the variation of the secondary coordination sphere, which leads to distinct distortion around the Co(II) ion, does not only modulate the single ion anisotropy of the complexes **1**–**3** but also the strength of intermolecular exchange interactions. This result is in line with the intermolecular exchange interactions determined by HF-EPR i.e. the observed interaction for **1** is stronger compared to that of **2**, as further described below.

Figure 2 shows the packing diagram of the representative complex **1**. It is found that there are four crystallographically equivalent molecules (symmetry code: -X, 0.5 + Y, 0.5-Z; labelled as Co(II)1-Co(II)4 in Fig. 2) within one unit cell. A pair of molecules labelled Co(II)1 and Co(II)2 in Fig. 2 generates another pair labelled Co(II)3 and Co(II)4, respectively by inversion symmetry. Although, the molecules Co(II)1 and Co(II)2 (and their symmetrically equivalent molecules) are crystallographically equivalent (Fig. 2), they do not overlay on top of each other, i.e. the molecule Co(II)2 is slightly tilted away from the molecule Co(II)1. This leads to a small angle of 14.8° between the anisotropy axes of the respective molecules. Fig. 2 also shows the Co(II)…Co(II) distances between the molecules within the unit cell (6.98, 10.40 and 11.63 Å). A more detailed description of the crystal structure of **1**, as well as those of **2** and **3**, is given in Ref. [37]. The strongly different distances between the Co(II) ions already implies a hierarchy of the possible intermolecular exchange interactions. In particular, magnetic coupling between the further separated molecules, with intermolecular distances of 10.40 and 11.63 Å, is expected to be extremely weak or negligible. A more detailed discussion regarding the possible coupling pathways between the Co(II) ions is given below.

3.1. Magnetic anisotropy and crystal field

To determine the SH parameters of **1**–**3** quantitatively, tuneable HF-EPR studies were performed. The measured spectra of the investigated materials display clear resonance features in the frequency and magnetic field range under study. Depending on the measurement frequency, up to four different resonances are observed at $T = 2$ K, as shown in Fig. 3. The spectra obtained for **1** and **2** exhibit strong field-dependent mixing of the phase and amplitude signals, which prevents appropriate phase correction of the spectra. However, as the experimental setup enables the detection of both the phase and amplitude of the transmitted microwave radiation, the actual resonance fields can be well read from the data, which enables the precise determination of the resonance field at a given frequency.

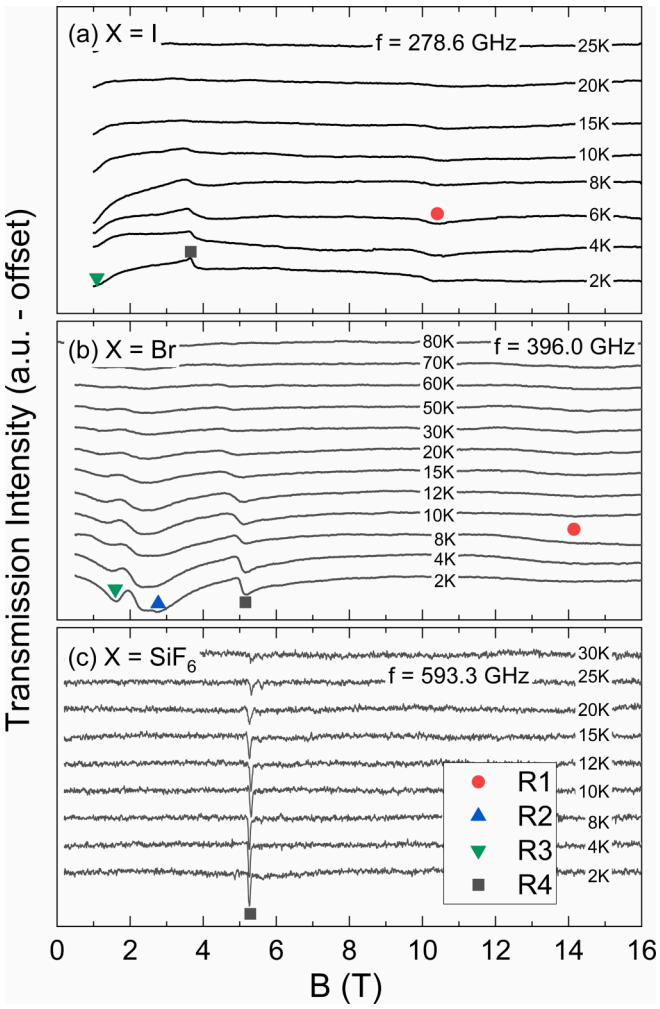

Fig. 3. HF-EPR spectra at different temperatures for (a) complex **1** at $\nu = 278.6$ GHz (9.3 cm^{-1}) (data from Ref. [37]), (b) **2** at $\nu = 396.0$ GHz (13.2 cm^{-1}) and (c) **3** at $\nu = 596.3$ GHz (19.9 cm^{-1}). The symbols denote different resonance features associated with the respective branches R1 to R4 in Fig. 5.

Figure 3(c) shows one sharp resonance for **3** at the frequency $\nu =$ 593.3 GHz in the field range under study (0 – 16 T). Upon heating, this feature is visible up to 30 K, but becomes weaker, indicating Curie-like behaviour, i.e., the feature is associated with a ground state resonance. Notably, a small side feature appears (see, e.g., the spectrum at $T = 25$ K), which is discussed below. Complex **2** features four resonances at $\nu =$ 396.0 GHz, labelled R1 to R4. Again, R2 to R4 are ground state resonances while R1 shows an activated behaviour, as indicated by the observed temperature dependence. The positions of the obtained resonance features for all three investigated complexes are shown in the frequency vs magnetic field diagrams (see Fig. 4). Data for **1** have been reported previously [37] and are presented for comparison purposes with the other structurally analogous complexes. Note, that the resonance branch R1 of **1** displays an activated behaviour similar to R1 of **2** as demonstrated by the temperature dependence of the associated

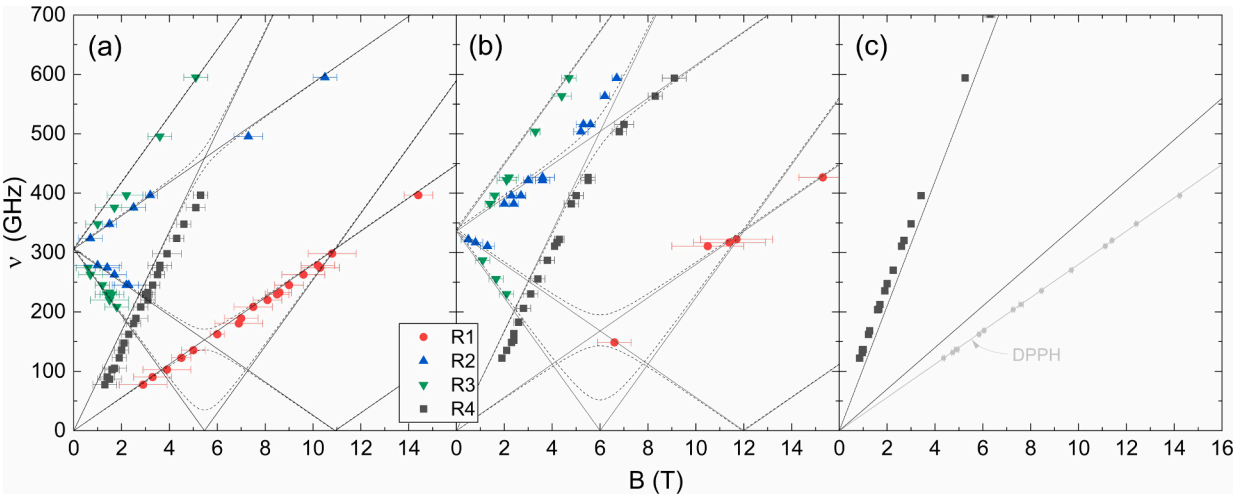

Fig. 4. Frequency vs. magnetic resonance field diagram of complex **1** (a, experimental data from Ref.[37]), **2** (b) and **3** (c) measured at $T = 2$ K. The solid black lines correspond to a simulation using the SH shown in Eqn. (3) with the parameters listed in Table 1 and without transversal anisotropy (i.e., $E = 0$). Dashed lines visualize the influence of a finite value for E ($E = 10$ GHz (0.33 cm^{-1}) for **1** and $E = 15$ GHz (0.50 cm^{-1}) for **2**).

Table 1
Simulation parameters using the SH shown in Eqn. (3) extended by an exchange coupling term as shown in Eqn. (1). The third column provides an upper limit of finite E for **1** and **2**.

Complex	D (GHz)	$\|E\|$ (GHz)	g_z	J (GHz)
1	−153(2)	≤10	2.00(5)	−5.5(5)
2	−168(5)	≤15	2.00(10)	−4.1(5)
3	< −400	≠ 0	2.65(1)	+3.5(2)

resonance features [37].

The measured resonance positions can be summarised in distinct branches. For **1** and **2**, four branches R1 to R4 are found, while only one branch is observed for **3** (see Fig. 4). Branches R1 and R4 in **1** and **2** as well as the single resonance branch in **3** display linear behaviour and exhibit no excitation gap (Δ) at $B = 0$ T. We conclude that the associated transitions appear within the Kramers doublets $m_S = \pm 1/2$ and $\pm 3/2$. In contrast, R2 and *R*3 in both **1** and **2** show gaps at zero field of>300 GHz (10 cm^{-1}) indicating splitting of the associated spin states, i.e. the so-called zero-field splitting (ZFS) [58]. Finite ZFS can be attributed to magnetic anisotropy due to the crystal field induced by the surrounding ligands.

Effective *g*-values can be extracted from the slope of the branches. Since the powder crystallites are aligned with respect to the external field, only one component of the in general anisotropic *g*-factor is measured, which is denoted here as g_z. Note, that g_z is explicitly not meant as the g_{zz} component of the *g*-tensor, since g_{zz} and D_{zz} are not in parallel but tilted based on NEVPT2 calculations on the representative complex **1** (see Figure S6 and Ref. [37]). The slopes of the branches R1 and R2 in **1** and **2** imply $g_z = 2.00(5)$ and $g_z = 2.0(1)$, respectively. The features are hence associated with transitions $\Delta m_S = \pm 1$. In contrast, R3 and R4 show much steeper slopes with $g_z = 4.0(1)$ and $g_z = 6.0(1)$, respectively, indicating forbidden transitions, i.e., $\Delta m_S = \pm 2$ and ± 3. The slope of the single branch observed in **3** indicates $g_z = 7.5(1)$. A quantitative analysis of the data applies the effective SH in Eqn. (3), which describes the Co(II) centres as well isolated spins $S = 3/2$ featuring axial and transversal anisotropy, D and E. In addition to axial and transversal anisotropy terms, the SH includes the Zeeman term with the Bohr magneton μ_B and the external magnetic field B [42].

$$H = g\mu_B \vec{B} \bullet \vec{S} + D\left[S_z^2 - \frac{S(S+1)}{3}\right] + E\left(S_x^2 - S_y^2\right) \quad (3)$$

A simulation of the resonance branches using Eqn. (3) with the parameters given in Table 1 and $E = 0$ yields good agreement to the experimental data, as shown in Fig. 4 as solid black lines. As mentioned above, there are two different orientations of the anisotropy axis within the crystal structure. Consequently, the anisotropy axis of the oriented powder is 7.4° tilted away from the magnetic field direction. However, as can be seen in Figure S1, this leads only to marginal effects on the branches in the low field region (below 8 T), where most of the HF-EPR data have been acquired.

Note, there is a slight discrepancy of the modes R4 (black squares), which is discussed below. For complex **3**, only one (forbidden) Kramers resonance is observable, which excludes quantitative determination of the axial anisotropy but implies $|D| > 400$ GHz (13.3 cm^{-1}). However, considering the high measured g_z value of this complex, the real *D*-anisotropy can be much higher than this lower boundary which is given by the accessible frequency range of the spectrometer. The obtained *D*-

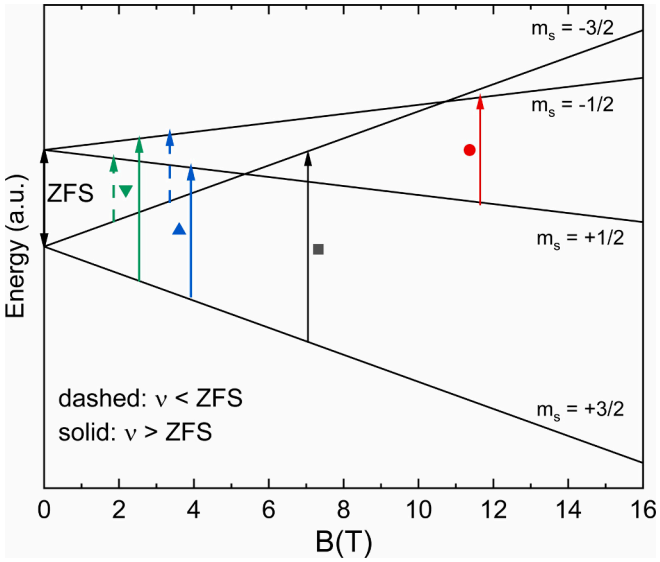

Fig. 5. Energy-level diagram using Eqn. (3) with $S = 3/2$, $D < 0$, and $E = 0$. The external field is oriented along the direction of the anisotropy axis. Coloured arrows mark transitions between the spin states of the correspondingly marked resonance branches (cf. Figs. 3 and 4). Solid arrows show transitions at measurement frequencies $\nu > \Delta/h$, i.e. larger than the zero-field gap, dashed arrows are associated with $\nu < \Delta/h$.

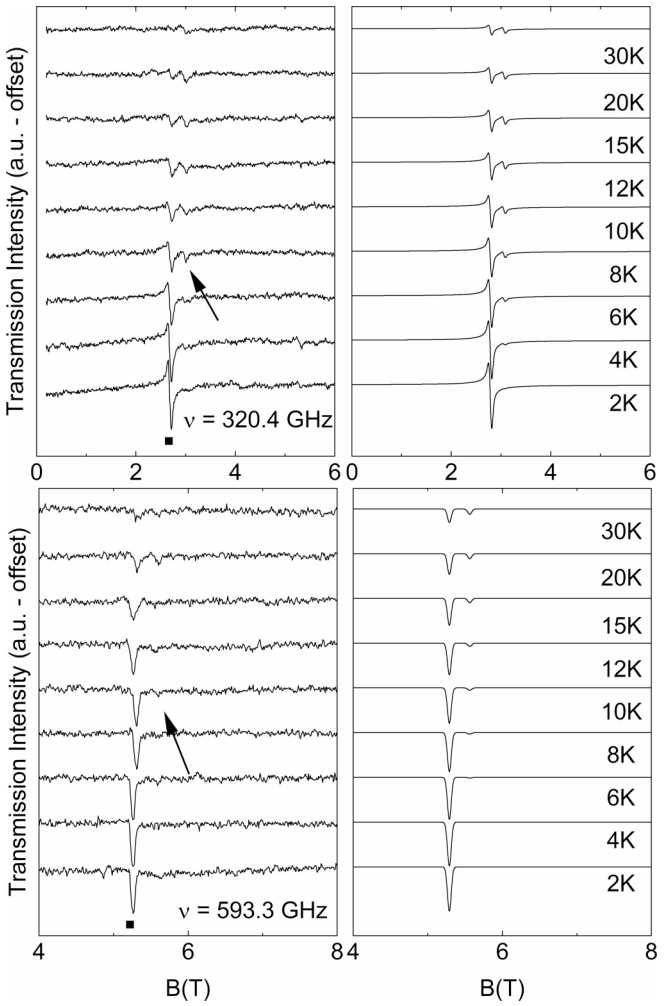

Fig. 6. HF-EPR spectra of complex **3** at different temperatures measured at (a) $\nu = 320.4$ GHz and (c) 593.3 GHz. Arrows indicate the appearance of an extra feature with rising temperatures. (b) and (d) show simulations at each frequency and temperature, respectively, employing $g_z = 2.65$, $J = 3.5$ GHz (0.11 cm^{-1}) and $|E| > 0$ GHz (see the text).

values for all three investigated samples are in good agreement with the ones obtained from the fit of the dc magnetisation data and they show the same tendency as the respective heights predicted by DFT calculations reported earlier [37].

While $|D|$ is deduced from the simulation of the resonance branches, for experimental determination of the sign of D the temperature dependence of the resonance intensities and/or the relative intensities of the different features at low temperatures must be considered. Except for R1 and R3 in **1** as well as R1 in **2**, all the observed features in Fig. 3 show a Curie-like behaviour, indicating ground state transitions [59]. The other branches show activated behaviour, implying that the initial state of the transition is not a ground state but energetically gapped at $B = 0$ T. These observations evidence a negative sign of D, as seen in the corresponding energy-level diagram visualising the results of our simulations in the case $D < 0$ (Fig. 5). The experimentally observed transitions obtained at frequencies above (below) the ZFS gap Δ/h are visualised by solid (dashed) coloured arrows. The red and black branches in Fig. 5 can be assigned to transitions within the $m_S = \pm 1/2$ and $\pm$ 3/2 Kramers doublets, respectively, whereas the green and blue branches correspond to gapped transitions between the mentioned doublets. Due to the negative sign of D, the $S = 3/2$ Kramers doublet is shifted to lower energies relative to the $S = 1/2$ doublet. The fact that R4 in **1** is more pronounced than R1 further corroborates the negative sign of the single-ion anisotropy parameter. We also recall the observed almost linear behaviour of the resonance branches shown in Fig. 4, which indicates a preferential orientation of the anisotropy axis along the direction of the external magnetic field and by this, a negative sign of the anisotropy [60,61].

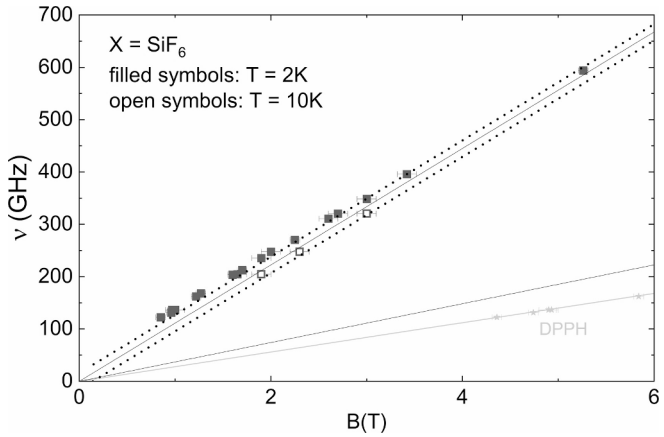

Fig. 7. Frequency vs. magnetic field diagram of complex **3**. Closed symbols mark the main branch which is observable at $T = 2$ K, open symbols show the additional high temperature feature at $T = 10$ K. Solid lines correspond to a simulation using a monomeric approach for the Co(II) ions, dotted lines simulate the dimeric model explained in the main text. The light grey branch shows the DPPH standard to ensure the magnetic field and frequency calibration, and by this the resonance positions.

Our data clearly show forbidden transitions, i.e. transitions with $\Delta m_S > 1$, which are not supposed to be detected in the strict case of $E = 0$ and aligned crystallites. Since our data evidence aligned crystallites, we conclude a mixing of states induced by finite transversal anisotropy. In order to assess the effect of a finite E value, simulation results employing $E > 0$ are shown in Fig. 4 by dashed lines. Expectedly, the associated resonance branches feature anti-crossing and gap formation. Comparing the simulations in the regions of anti-level crossing with the experimental data enables the establishment of upper limits for E in the case of complexes **1** and **2**, which are given in Table 1. For **3**, only the forbidden resonance branch within the lower $S = 3/2$ Kramers doublet is observed in our measurement range below 750 GHz (25 cm^{-1}), which obviates estimating E. However, the fact that the forbidden transition is clearly observed implies finite transversal anisotropy.

3.2. Exchange coupling

In addition to the features discussed above, the rather sharp resonance observed in **3** (as compared to **1** and **2**) enables the detection of an extra resonance at elevated temperatures which is not captured by the SH in Eqn. (3). Upon heating, the spectra measured at $\nu = 320.4$ and 593.3 GHz show the evolution of a distinct second feature in the vicinity of resonance R4 (Fig. 6). The resonance positions of the extra features at $T = 10$ K are shown by open symbols in Fig. 7, while the low-temperature resonances are displayed by filled markers. Identical slopes of the two branches imply equal effective g-values. As demonstrated in Fig. 7 by solid black lines, the elevated temperature features are not captured by the monomer model discussed above. We hence attribute it to the presence of weak intermolecular coupling between neighbouring spins. We note that dipolar interactions should lead to a broadening of the resonance line since they are assumed to prevail between all the Co(II) ions, but not to the appearance of two well separated resonance features, as observed in Fig. 6. Additionally, the calculated dipolar coupling strength between the nearest neighbouring Co(II) centres is in the range of 0.1 GHz, which is almost two orders too small to account for the observed zero field splitting.

Expanding the single molecule simulation by intermolecular

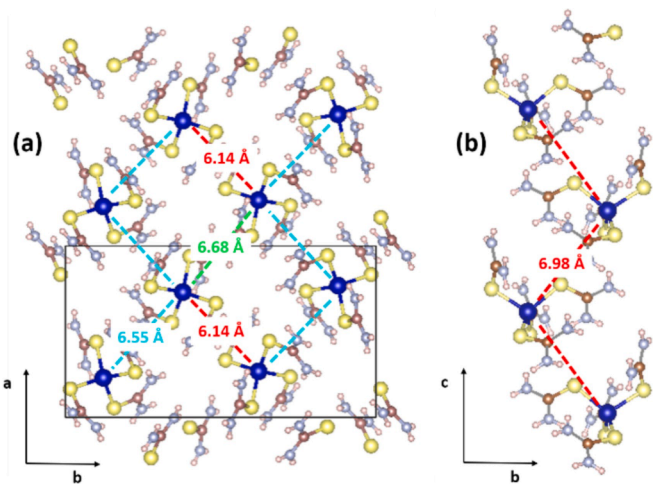

Fig. 8. Structural arrangement of the molecules in the *ab*-plane of complex **3** (a) as well as the chain-like arrangement along the c-direction for complexes **1** and **2** (b). Blue = Co(II), yellow = S, light blue = N, brown = C and white = H. Different intermolecular Co(II)···Co(II) distances are marked by differently coloured dashed lines. Only the molecules with the shortest Co(II)···Co(II) distances are shown. We refer to Ref. [37] for a complete structural description.

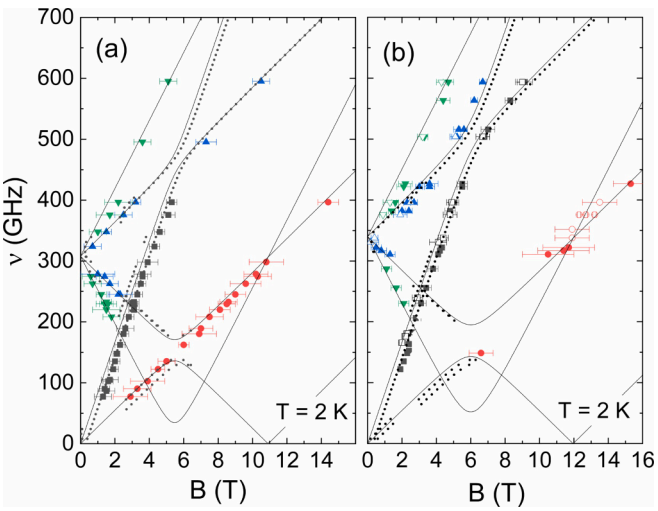

Fig. 9. Frequency vs. magnetic field diagram of complexes **1** (a) and **2** (b). The dotted lines show simulations using the SH in Eqn. (1) extended by finite exchange coupling (see the text) between two neighbouring spins. *D* and *E* anisotropy parameters as well as g_z-values equal those of the single-ion model represented by the solid lines (cf. Table 1). The open symbols in panel (b) represent the resonance branches observed in a magnetically diluted sample of **2**.

exchange interactions mediated via the ligands straightforwardly captures the existence of the additional resonance feature, as visualised in the energy-level diagram shown in Figure S2. Specifically, the presence of one extra feature can be phenomenologically explained by an isotropic dimer-like exchange coupling *J* between two neighbouring sites [62]. The dimer model serves as a minimal model to describe the experimental observations. Indeed, the structure of **3** shows rather short Co(II)–Co(II) distances in the range 6 to 6.5 Å in the *ab*-plane (see Fig. 8 (a)), while the inter-plane distances are considerably larger. Furthermore, as can be seen in Fig. 8(a), the in-plane distances between the Co (II) ions are not equivalent. The shortest distance between the Co(II) ions in the *ab*-plane amounts to 6.14 Å, while the other nearest neighbors distances are at least 6.55 Å which, from a phenomenological point of view, tentatively motivates a dimer-like scenario, which is found to describe our HF-EPR results. Our numerical studies presented below confirm this scenario.

The exchange Hamiltonian corresponding to a dimer interaction is shown in Eqn. (1). Simulating the spectra at $\nu = 320.4$ and 593.3 GHz at various temperatures using the extended (i.e., Eqn. (3) + Eqn. (1)) model yields a good description of both the resonance positions and the spectral intensities, as shown in Fig. 6 (b) and (d). Employing $g_z = 2.65$ and $E > 0$ GHz, our analysis yields ferromagnetic intermolecular coupling $J = 3.5(2)$ GHz (0.110(6) cm^{-1}). This value is in line with the intermolecular couplings found in other high-spin Co(II) compounds [63]. Note, due to the fact that only one resonance branch is detected, no relative intensities between the resonance features, and by this no proper *E*-value, can be quantised. For the simulation, an arbitrary *E*-value with $|E| > 0$ was used.

The broad resonance lines prevent the identification of the corresponding extra features in **1** and **2**, however the similar Co(II)···Co(II) distances in all the samples under investigation suggest that intermolecular coupling is to be expected, too. Indirect evidence is obtained from the temperature dependence of R4 (depicted by the black square in Fig. 3) in complexes **1** and **2**, which clearly shifts to lower fields upon heating (see Figure S3). We attribute this shift to a merging of the main feature with an additional one showing up at the low field side. Notably, this shift is opposite to the additional high-temperature peak observed in **3,** which suggests a different sign of *J*, i.e., an antiferromagnetic intermolecular interaction.

In contrast to **3**, the structures of **1** and **2** imply the shortest Co(II)··· Co(II) distance of 6.98 Å in the bc-plane(see Fig. 2), while the other distances are much larger. As shown in Fig. 8(b), this yields a zig-zag chain structure with a tilted nature, which may again contribute to the dimer-like magnetic scenario. While our numerical calculations, due to very small interactions, do not discriminate between a uniform or alternating chain scenario, our experimental data are well described by the latter one, e.g. a dimer-like or weakly interacting dimer model as the distinct thermally activated resonance line is not expected in a 1D model [64,65].

The presence of a finite antiferromagnetic interaction indeed explains the discrepancy of the experimental data and the model in Fig. 4, where the resonance branches R4 are not perfectly described by the simulation. As seen in Fig. 4, the experimental data are overall shifted with respect to the simulated branch yielding a seemingly negative Δ in **1** and **2**. This shift is accounted for by the intermolecular exchange interaction. Quantitatively, the experimental data are described by the extended model with $J = -5.5(5)$ GHz (-0.18 cm^{-1}) for **1** and $-4.1(5)$ GHz (-0.13 cm^{-1}) for **2**, as seen in Fig. 9. The difference, i.e. positive sign of *J* in **3** implying a ferromagnetic intermolecular interaction, is clearly evidenced by the fact that the corresponding low-temperature branch in **3** exhibits a positive Δ value. Note, that the resonance positions have been confirmed by a DPPH marker.

In order to prove the relevance of the intermolecular effects, additional studies on a diluted sample of **2** have been performed, using a non-magnetic matrix solvent [37]. The resonance features obtained on the diluted sample, shown as open symbols in Fig. 9(b), confirm a much smaller intermolecular coupling by an almost vanishing shift of R4. A direct comparison of an exemplary spectrum obtained at same frequencies for 100 % and diluted 25 % samples of **2**, shown in Figure S4, clearly demonstrates a dilution dependent shift of around 0.5 T. Measurements on diluted samples of **1** and **3** were not successful. However, as stated earlier, **1** is structurally analogous to **2** and hence the same phenomenon observed for **2** can be extended to **1**.

3.3. *Hirshfeld surface analysis of complexes 1–3*

One of the important aspects of this report is the quantitative determination of the strength of the intermolecular interactions in **1**–**3** using HF-EPR (*vide infra*). To understand the inter- and intramolecular interactions observed in the solid-state of these complexes, a Hirshfeld

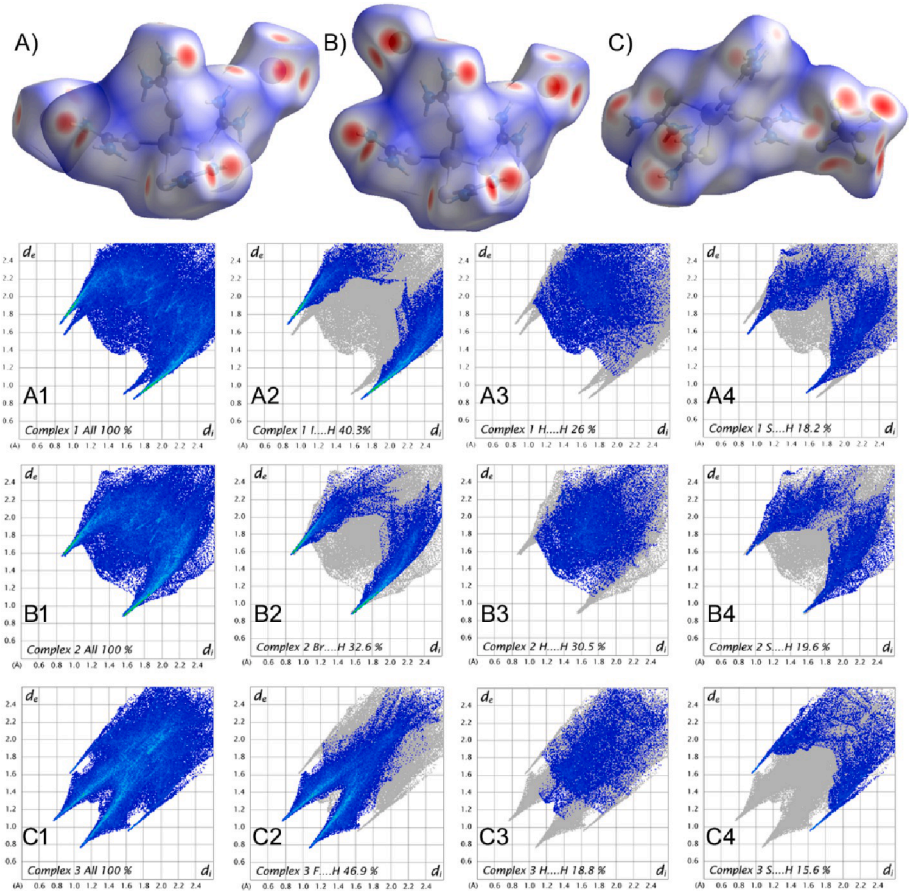

Fig. 10. Hirshfeld surface analysis mapped with d_{norm} for complexes **1** (panel A), **2** (Panel B) and **3** (panel C). The red colours indicate contacts with distances shorter than the van der Waals radii, i.e. very weak inter- or intramolecular interactions. Two-dimensional (2D) fingerprint plots are shown for the cation of complex **1**, where d_i is the distance from the Hirshfeld surface to the nearest atom inside the surface and d_e is the distance from the nearest atom outside the surface. Total intermolecular contacts including reciprocal contacts in **1**: (A1) 100% contacts, (A2) the relative percentage of I···H contacts (40.3%), (A3) H···H contacts (26 %), (A4) S···H contacts (18.2 %), **2**: (B1) 100% contacts, (B2) the relative percentage of Br···H contacts (32.6%), (B3) H···H contacts (22.4%,), (B4) S···H contacts (19.6 %), **3**: (C1) 100% contacts, (C2) the relative percentage of F···H contacts (46.9 %), (B3) H···H contacts (18.8 %,), (B4) S···H contacts (15.6 %). The intermolecular contacts including reciprocal contacts with < 5 % in all the complexes are not shown.

analysis was carried out (see Fig. 10). The Hirshfeld surface of all the three complexes shows that the intermolecular interactions between the molecules are mediated predominantly through the halide (anions in the crystal lattice) and hydrogen atoms of the thiourea ligand bound to the Co(II) ion. The various regions of color on these surfaces describe the inter- and intramolecular contacts present in their crystal structures. Two-dimensional (2D) fingerprint plots (Fig. 10, panels A1-C4) were also generated for all the complexes and used to visualize supramolecular features, such as weak inter- and intramolecular interactions and close contacts, as seen in their crystal structures. Both the Hirshfeld surface and fingerprint plots were extracted from the d_i and d_e values using *CrystalExplorer* [66,67], where d_i represents the distance from the Hirshfeld surface to the nearest atom inside the surface and with d_e being the distance from the nearest atom outside the surface [68]. The results of these plots indicate that the percentage of intermolecular X···H (where X = I (**1**), Br (**2**) and F (**3**)) contacts are 40.3 % in **1**, 32.6 % in **2,** and 46.9 % in **3** of the total share. The other significant contributions, including reciprocal contacts, are H···H and S···H, having relative contributions of 26 %, and 18.2 % in **1**; 30.5 % and 19.6 % in **2**, and 18.8 % and 15.6 % in **3**, respectively. As **1** and **2** are structurally analogous to each other, the relative percentage interaction of I···H is larger in **1** compared to the Br···H interaction in **2**. Hence, the overall exchange strength is expected to be stronger in **1** compared to **2**, which is in excellent agreement with the experimental observation (*vide infra*).

3.4. Numerical calculation for estimating the exchange interactions

Experimentally, there is an antiferromagnetic intermolecular exchange interaction between the molecules in the crystal lattice of **1** or **2**, while a ferromagnetic intermolecular exchange interaction was shown within **3**. To shed light on the mechanism of the intermolecular exchange interactions, beyond the phenomenological comparison of intermolecular distances, DFT calculations were performed on the representative complex **1**. As stated earlier, **1** possesses both intra- and intermolecular hydrogen-bonding (H-bonding) [37]. Existence of super-exchange interactions between monomeric Cu(II), Fe(II), Fe(III) and Co(III)-Cr(III), V(IV)-Cu(II) ions etc. mediated via H-bonding is well established in literature by Alvarez and co-workers, and experimentally proven for certain Co(II) systems [55,56,69,70]. Besides the thematization of H-bondings, they have also proposed a methodology to mitigate the intermolecular exchange interaction (ferro- or antiferromagnetic) by crystal engineering [5,7,8].

As shown in Fig. 2, the intermolecular distance between the molecules is different in different directions for **1**. Three different J_s values based on the internuclear distances (J_1: Co(II)···Co(II) = 6.98 Å, J_2: 10.40 Å and J_3: 11.63 Å, see Fig. 2) are defined within the crystal lattice of **1** as coupling directions in a dimeric model for computing the exchange interaction. Our calculations predict that the exchange interaction between all the pairs of the binuclear system is antiferromagnetic in complex **1**. DFT calculations yield $J_1 = -0.08\ cm^{-1}$, $J_2 = -0.001\ cm^{-1}$ and $J_3 = 0\ cm^{-1}$.

It is found, that the J_1 interaction is strongest, while the other two are negligible. Thus, not only the distance dependent dipolar interactions, but also the intermolecular exchange interactions show a clear hierarchy in favour of J_1. The latter can be explained by a strong intermolecular I or S···H—N interaction (2.65 Å). Furthermore, a relatively strong antiferromagnetic coupling is evidenced from the SOMOs (see Figure S5 in ESI) [55,56,69,70].

Although the nature of the exchange interaction is predicted correctly, the magnitude of the computed *J* values are different from the experimentally extracted ones, and this may be attributed to relatively smaller intermolecular interactions, which are extremely challenging to

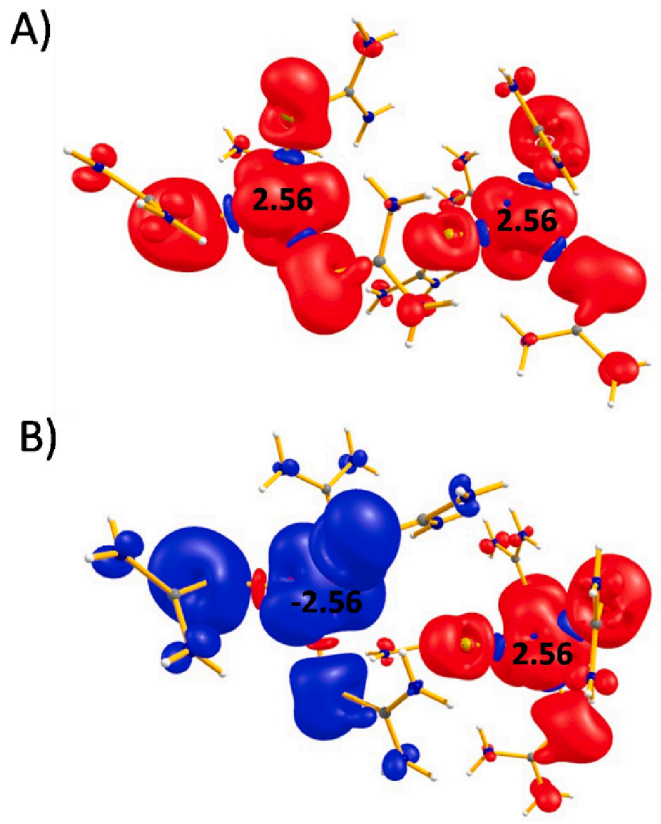

Fig. 11. DFT computed spin density plots of A) the high-spin state and B) the broken symmetry model of complex **1**. Spin densities are plotted using an isosurface value of 0.001 e/bohr^3.

capture accurately by DFT methods. The spin density plot for the high-spin (HS) and broken symmetry (BS) models corresponding to J_1 reveal strong delocalisation of spin density on the ligands, propagating relatively stronger intermolecular exchange interactions as shown in Fig. 11. A closer inspection reveals a small but non-negligible spin density on the H-atom involved in the H-bonding interactions, supporting our aforementioned claim [70].

4. Conclusions

A sophisticated HF-EPR methodology was employed to quantitatively determine the Spin Hamiltonian parameters on a family of high spin Co(II) complexes $[Co(L_1)_4]X_2$ where X = I (**1**), Br (**2**) and $[Co(L_1)_4]SiF_6$ (**3**), which also establishes the presence of non-zero E values in all the complexes. The study presented here furnishes the experimental proof for a sizable influence of the secondary coordination sphere on the magnitude of the axial anisotropy parameter D, which was measured directly by HF-EPR for complexes **1**–**3**. Further, intermolecular antiferromagnetic exchange interactions for **1** ($J = -5.5(5)$ GHz (-0.18 cm^{-1}) and **2** ($J = -4.1(5)$ GHz (-0.13 cm^{-1})) were found, while a ferromagnetic exchange interaction was noticed for **3** (J = 3.5(2) GHz (0.11 cm^{-1})). The presence of a very weak exchange interaction between the molecules of **1** was also confirmed by theoretical calculations. Overall, this study discloses SH parameters accurately using HF-EPR and that through crystal engineering (by changing the anions the supramolecular interactions can be controlled) one can modulate not only the axial anisotropy but also intermolecular interaction pathways. This is an unconventional, yet a versatile approach that will pave the way to reveal a new generation of Co(II) complexes with fascinating magnetic properties.

CRediT authorship contribution statement

Lena Spillecke: Writing - original draft, Investigation, Formal analysis. **Shalini Tripathi:** Investigation, Resources, Formal analysis. **Changhyun Koo:** Supervision, Writing - original draft, Writing - review & editing. **Mursaleem Ansari:** Resources, Formal analysis. **Shefali Vaidya:** Resources, Formal analysis. **Amaleswari Rasamsetty:** Formal analysis. **Talal Mallah:** Writing - review & editing. **Gopalan Rajaraman:** Writing - review & editing, Formal analysis. **Maheswaran Shanmugam:** Conceptualization, Supervision, Writing - review & editing. **Rüdiger Klingeler:** Conceptualization, Supervision, Writing - original draft, Writing - review & editing.

Declaration of Competing Interest

The authors declare that they have no known competing financial interests or personal relationships that could have appeared to influence the work reported in this paper.

Acknowledgements

Funding by Bundesministerium für Forschung und Bildung via project SpinFun (13XP5088) is gratefully acknowledged. L.S. acknowledges support by Landesgradiertenförderung via the research training group Basic building blocks for quantum enabled technologies and C.K. by Deutsche Forschungsgemeinschaft (DFG) through grant KO 5480/1-1. MS thanks the funding agencies SERB (CRG/2019/004185/SPR/2019/001145), CSIR (01(2933)/18/EMR-II) and IIT Bombay for financial support. G.R. thanks SERB for funding (Grant CRG/2018/000430; DST/SJF/CSA-03/2018-10; SB/SJF/2019-20/12).

Appendix A. Supplementary data

Supplementary data to this article can be found online at https://doi.org/10.1016/j.poly.2021.115389.

References

[1] K.M. Mertes, Y. Suzuki, M.P. Sarachik, Y. Myasoedov, H. Shtrikman, E. Zeldov, E. M. Rumberger, D.N. Henrickson, G. Christou, Mn_{12}-acetate: a prototypical single molecule magnet, Solid State Commun. 127 (2003) 131–139.
[2] H. Oshio, M. Nakano, High-spin molecules with magnetic anisotropy toward single-molecule magnets, Chem. Eur. J. 11 (18) (2005) 5178–5185.
[3] R. Sessoli, D. Gatteschi, A. Caneschi, M.A. Novak, Magnetic bistability in a metal-ion cluster, Nature 365 (6442) (1993) 141–143.
[4] A.K. Bar, C. Pichon, J.-P. Sutter, Magnetic anisotropy in two- to eight-coordinated transition–metal complexes: Recent developments in molecular magnetism, Coord. Chem. Rev. 308 (2016) 346–380.
[5] G.A. Craig, M. Murrie. 3d single-ion magnets, Chem. Soc. Rev., 10.1039/C4CS00439F, 44 (2015) 2135-2147.
[6] M.S. Fataftah, J.M. Zadrozny, D.M. Rogers, D.E. Freedman, A mononuclear transition metal single-molecule magnet in a nuclear spin-free ligand environment, Inorg. Chem. 53 (19) (2014) 10716–10721.
[7] D.E. Freedman, W.H. Harman, T.D. Harris, G.J. Long, C.J. Chang, J.R. Long, Slow Magnetic Relaxation in a High-Spin Iron(II) Complex, J. Am. Chem. Soc. 132 (4) (2010) 1224–1225.
[8] N. Ishikawa, M. Sugita, T. Ishikawa, S.-y. Koshihara, Y. Kaizu, Lanthanide double-decker complexes functioning as magnets at the single-molecular level, J. Am. Chem. Soc. 125 (29) (2003) 8694–8695.
[9] Y. Rechkemmer, F.D. Breitgoff, M. van der Meer, M. Atanasov, M. Hakl, M. Orlita, P. Neugebauer, F. Neese, B. Sarkar, J. van Slageren, A four-coordinate cobalt(II) single-ion magnet with coercivity and a very high energy barrier, Nat. Commun. 7 (2016) 10467.
[10] D. Tu, D. Shao, H. Yan, C. Lu. A carborane-incorporated mononuclear Co(ii) complex showing zero-field slow magnetic relaxation, Chem. Commun. 52 2016 14326-14329. 10.1039/C6CC07728E.
[11] J.M. Zadrozny, J.R. Long, Slow magnetic relaxation at zero field in the tetrahedral complex $[Co(SPh)_4]^{2-}$, J. Am. Chem. Soc. 133 (51) (2011) 20732–20734.
[12] D.S. Krylov, F. Liu, S.M. Avdoshenko, L. Spree, B. Weise, A. Waske, A.U.B. Wolter, B. Büchner, A.A. Popov, Record-high thermal barrier of the relaxation of magnetization in the nitride clusterfullerene $Dy_2ScN@C_{80}$-I_h, Chem. Commun. 53 (56) (2017) 7901–7904.
[13] D. Tanaka, T. Inose, H. Tanaka, S. Lee, N. Ishikawa, T. Ogawa, Proton-induced switching of the single molecule magnetic properties of a porphyrin based TbIII

double-decker complex, Chem. Commu. 48 (63) (2012) 7796, https://doi.org/10.1039/c2cc00086e.
[14] C. Das, A. Upadhyay, S. Vaidya, S.K. Singh, G. Rajaraman, M. Shanmugam, Origin of SMM behaviour in an asymmetric Er(iii) Schiff base complex: a combined experimental and theoretical study, Chem. Commu. 51 (2015) 6137–6140.
[15] P. Cieslik, P. Comba, W. Hergett, R. Klingeler, G.F.P. Plny, L. Spillecke, G. Velmurugan, Molecular magnetic properties of a dysprosium(III) complex coordinated to a nonadentate bispidine ligand, Z. Anorg. Allg. Chem. 647 (8) (2021) 843–849.
[16] M. Atanasov, D. Aravena, E. Suturina, E. Bill, D. Maganas, F. Neese, First principles approach to the electronic structure, magnetic anisotropy and spin relaxation in mononuclear 3d-transition metal single molecule magnets, Coord. Chem. Rev. 289-290 (2015) 177–214.
[17] S. Gomez-Coca, E. Cremades, N. Aliaga-Alcalde, E. Ruiz, Mononuclear Single-Molecule Magnets: Tailoring the Magnetic Anisotropy of First-Row Transition-Metal Complexes, J. Am. Chem. Soc. 135 (2013) 7010–7018.
[18] Y.-Y. Zhu, C. Cui, Y.-Q. Zhang, J.-H. Jia, X. Guo, C. Gao, K. Qian, S.-D. Jiang, B.-W. Wang, Z.-M. Wang, S. Gao, Zero-field slow magnetic relaxation from single Co (ii) ion: a transition metal single-molecule magnet with high anisotropy barrier, Chem. Sci. 4 (2013) 1802–1806.
[19] Z.-Y. Ding, Y.-S. Meng, Y. Xiao, Y.-Q. Zhang, Y.-Y. Zhu, S. Gao, "Probing the influence of molecular symmetry on the magnetic anisotropy of octahedral cobalt (ii) complexes," Inorg. Chem. Front., 10.1039/C7QI00547D, 4, (2017), 1909-1916.
[20] D. Schweinfurth, J. Krzystek, M. Atanasov, J. Klein, S. Hohloch, J. Telser, S. Demeshko, F. Meyer, F. Neese, B. Sarkar, Tuning magnetic anisotropy through ligand substitution in five-coordinate Co(II) complexes, Inorg. Chem. 56 (9) (2017) 5253–5265.
[21] S. Tripathi, A. Dey, M. Shanmugam, R.S. Narayanan, V. Chandrasekhar, Cobalt(II) Complexes as Single-Ion Magnets, in: V. Chandrasekhar, F. Pointillart (Eds.), Organometallic Magnets, Springer International Publishing, Cham, 2019, pp. 35–75.
[22] G. Peng, Y. Chen, B. Li, Y.-Q. Zhang, X.-M. Ren, Bulky Schiff-base ligand supported Co(ii) single-ion magnets with zero-field slow magnetic relaxation, Dalton Trans. 49 (2020) 5798–5802.
[23] A. Świtlicka, B. Machura, M. Penkala, A. Bienko, D.C. Bienko, J. Titis, C. Rajnak, R. Boca, A. Ozarowski, Slow magnetic relaxation in hexacoordinated cobalt(ii) field-induced single-ion magnets, Inorg. Chem. Front. 7 (2020) 2637–2650.
[24] S. Tripathi, S. Vaidya, N. Ahmed, E. Andreasen Klahn, H. Cao, L. Spillecke, C. Koo, S. Spachmann, R. Klingeler, G. Rajaraman, J. Overgaard, M. Shanmugam, Structure-property correlation in stabilizing axial magnetic anisotropy in octahedral Co(II) complexes, Cell Rep. Phys. Sci. 2 (4) (2021) 100404, https://doi.org/10.1016/j.xcrp.2021.100404.
[25] W. Wernsdorfer, S. Bhaduri, C. Boskovic, G. Christou, D.N. Hendrickson, Spin-parity dependent tunneling of magnetization in single-molecule magnets, Phys. Rev. B 65 (18) (2002), https://doi.org/10.1103/PhysRevB.65.180403.
[26] M.R. Saber, K.R. Dunbar. Ligands effects on the magnetic anisotropy of tetrahedral cobalt complexes, Chem. Commun. 50 (2014) 12266-12269. 10.1039/C4CC05724D.
[27] E.A. Suturina, D. Maganas, E. Bill, M. Atanasov, F. Neese, Magneto-structural correlations in a series of pseudotetrahedral $[CoII(XR)_4]^{2-}$ single molecule magnets: an ab initio ligand field study, Inorg. Chem. 54 (2015) 9948–9961.
[28] S. Vaidya, S. Tewary, S.K. Singh, S.K. Langley, K.S. Murray, Y. Lan, W. Wernsdorfer, G. Rajaraman, M. Shanmugam. What controls the sign and magnitude of magnetic anisotropy in tetrahedral Cobalt(II) single-ion magnets?, inorg. chem. 55 (20216) 9564-9578.
[29] J.M. Zadrozny, J. Telser, J.R. Long, Slow magnetic relaxation in the tetrahedral cobalt(II) complexes $[Co(EPh)_4]^{2-}$ (EO, S, Se), Polyhedron 64 (2013) 209–217.
[30] M. Idešicová, J. Titiš, J. Krzystek, R. Boča, Zero-field splitting in pseudotetrahedral Co(II) complexes: a magnetic, high-frequency and -field EPR, and computational study, Inorg. Chem. 52 (2013) 9409–9417.
[31] T. Jurca, A. Farghal, P.-H. Lin, I. Korobkov, M. Murugesu, D.S. Richeson, Single-molecule magnet behavior with a single metal center enhanced through peripheral ligand modifications, J. Am. Chem. Soc. 133 (40) (2011) 15814–15817.
[32] X.-L. Mei, Y. Ma, L.-C. Li, D.-Z. Liao. Ligand field-tuned single-molecule magnet behaviour of 2p–4f complexes, Dalton Trans. 41 (2012) 505-511. 10.1039/C1DT11795E.
[33] S. Vaidya, A. Upadhyay, S.K. Singh. T. Gupta, S. Tewary, S.K. Langley, J.P.S. Walsh, K.S. Murray, G. Rajaraman, M. Shanmugam. A synthetic strategy for switching the single ion anisotropy in tetrahedral Co(ii) complexes, Chem. Commun. 51 (2015), 3739-3742. 10.1039/C4CC08305A.
[34] Y. Gil, L. Llanos, P. Cancino, P. Fuentealba, A. Vega, E. Spodine, D. Aravena, Effect of second-sphere interactions on the magnetic anisotropy of lanthanide single-molecule magnets: electrostatic interactions and supramolecular contacts, J. Phy. Chem. C 124 (9) (2020) 5308–5320.
[35] D. Maganas, S. Sottini, P. Kyritsis, E.J.J. Groenen, F. Neese, Theoretical analysis of the spin hamiltonian parameters in Co(II)S4 complexes, using density functional theory and correlated ab initio methods, Inorg. Chem. 50 (18) (2011) 8741–8754.
[36] K.S. Pedersen, L. Ungur, M. Sifrist, A. Sundt, M. Schau-Magnussen, V. Vieru, H. Mutka, S. Rols, H. Weihe, O. Waldmann, L.F. Chibotaru, J. Bendix, J. Dreiser. Modifying the properties of 4f single-ion magnets by peripheral ligand functionalisation, Chem. Sci. 5 2014 1650-1660. 10.1039/C3SC53044B.
[37] S. Tripathi, S. Vaidya, K.U. Ansari, N. Ahmed, E. Rivière, L. Spillecke, C. Koo, R. Klingeler, T. Mallah, G. Rajaraman, M. Shanmugam, Influence of a counteranion on the zero-field splitting of tetrahedral Cobalt(II) thiourea complexes, Inorg. Chem. 58 (14) (2019) 9085–9100.
[38] S. Vaidya, P. Shukla, S. Tripathi, E. Riviere, T. Mallah, G. Rajaraman, M. Shanmugam, Substituted versus naked thiourea ligand containing pseudotetrahedral cobalt(II) complexes: a comparative study on its magnetization relaxation dynamics phenomenon, Inorg. Chem. 57 (2018) 3371–3386.
[39] J. Wu, J. Jung, P. Zhang, H. Zhang, J. Tang, B. Le Guennic, Cis–trans isomerism modulates the magnetic relaxation of dysprosium single-molecule magnets, Chem. Sci. (2016) 3632-3639, https://doi.org/10.1039/C5SC04510J,7.
[40] Y.-Y. Zhu, Y.-Q. Zhang, T.-T. Yin, C. Gao, B.-W. Wang, S. Gao, A family of $Co^{II}Co^{III}_3$ single-ion magnets with zero-field slow magnetic relaxation: fine tuning of energy barrier by remote substituent and counter cation, Inorg. Chem. 54 (2015) 5475–5486.
[41] J. Telser, J. Krzystek, A. Ozarowski, High-frequency and high-field electron paramagnetic resonance (HFEPR): a new spectroscopic tool for bioinorganic chemistry, J. Biol. Inorg. Chem. 19 (2014) 297–318.
[42] D. Gatteschi, A.L. Barra, A. Caneschi, A. Cornia, R. Sessoli, L. Sorace, EPR of molecular nanomagnets, Coord. Chem. Rev. 250 (11-12) (2006) 1514–1529.
[43] I. Oyarzabal, J. Ruiz, E. Ruiz, D. Aravena, J.M. Seco, E. Colacio, Increasing the effective energy barrier promoted by the change of a counteranion in a Zn–Dy–Zn SMM: slow relaxation via the second excited state, Chem. Commun. 51 (2015) 12353–12356.
[44] E.A. Suturina, J. Nehrkorn, J.M. Zadrozny, J. Liu, M. Atanasov, T. Weyhermüller, D. Maganas, S. Hill, A. Schnegg, E. Bill, J.R. Long, F. Neese, Magneto-structural correlations in pseudotetrahedral forms of the $[Co(SPh)_4]^{2-}$ complex probed by magnetometry, MCD spectroscopy, advanced EPR techniques, and ab initio electronic structure calculations, Inorg. Chem. 56 (5) (2017) 3102–3118.
[45] S. Titos-Padilla, J. Ruiz, J.M. Herrera, E.K. Brechin, W. Wersndorfer, F. Lloret, E. Colacio, Dilution-triggered SMM behavior under zero field in a luminescent Zn_2Dy_2 tetranuclear complex incorporating carbonato-bridging ligands derived from atmospheric CO_2 fixation, Inorg. Chem. 52 (16) (2013) 9620–9626.
[46] C. Boskovic, R. Bircher, P.L.W. Tregenna-Piggott, H.U. Güdel, C. Paulsen, W. Wernsdorfer, A.-L. Barra, E. Khatsko, A. Neels, H. Stoeckli-Evans, Ferromagnetic and antiferromagnetic intermolecular interactions in a new family of Mn_4 Complexes With An Energy Barrier To Magnetization Reversal, J. Am. Chem. Soc. 125 (46) (2003) 14046–14058.
[47] Z.-B. Hu, Z.-Y. Jing, M.-M. Li, L. Yin, Y.-D. Gao, F. Yu, T.-P. Hu, Z. Wang, Y. Song, Important role of intermolecular interaction in Cobalt(II) single-ion magnet from single slow relaxation to double slow relaxation, Inorg. Chem. 57 (17) (2018) 10761–10767.
[48] F. Habib, I. Korobkov, M. Murugesu, Exposing the intermolecular nature of the second relaxation pathway in a mononuclear cobalt(ii) single-molecule magnet with positive anisotropy, Dalton Trans. 44 (2015) 6368–6373.
[49] P. Comba, M. Großhauser, R. Klingeler, C. Koo, Y. Lan, D. Müller, J. Park, A. Powell, M.J. Riley, H. Wadepohl, Magnetic interactions in a series of homodinuclear lanthanide complexes, Inorg. Chem. 54 (23) (2015) 11247–11258.
[50] S. Stoll, A. Schweiger, EasySpin, a comprehensive software package for spectral simulation and analysis in EPR, J. Magn. Reson. 178 (1) (2006) 42–55.
[51] R.M. Dickson, A.D. Becke, Basis-set-free local density-functional calculations of geometries of polyatomic molecules, J. Chem. Phys. 99 (5) (1993) 3898–3905.
[52] A. Schäfer, C. Huber, R. Ahlrichs, Fully optimized contracted Gaussian basis sets of triple zeta valence quality for atoms Li to Kr, J. Chem. Phys. 100 (8) (1994) 5829–5835.
[53] R. Calvo, EPR measurements of weak exchange interactions coupling unpaired spins in model compounds, Appl. Magn. Reson. 31 (1-2) (2007) 271–299.
[54] M.J. Frisch, G.W. Trucks, H.B. Schlegel, G.E. Scuseria, M.A. Robb, J.R. Cheeseman, G. Scalmani, V. Barone, G.A. Petersson, H. Nakatsuji, X. Li, M. Caricato, A.V. Marenich, J. Bloino, B.G. Janesko, R. Gomperts, B. Mennucci, HP. Hratchian, J.V. Ortiz, A.F. Izmaylov, JL. Sonnenberg, D. Williams-Young, F. Ding, F. Lipparini, F. Egidi, J. Goings, B. Peng, A. Petrone, T. Henderson, D. Ranasinghe, V.G. Zakrzewski, J. Gao, N. Rega, G. Zheng, W. Liang, M. Hada, M. Ehara, K. Toyota, R. Fukuda, J. Hasegawa, M. Ishida, T. Nakajima, Y. Honda, O. Kitao, H. Nakai, T. Vreven, K. Throssell, J. A. Montgomery, Jr., J.E. Peralta, F. Ogliaro, M.J. Bearpark, J.J. Heyd, E.N. Brothers, K.N. Kudin, V.N. Staroverov, T.A. Keith, R. Kobayashi, J. Normand, K. Raghavachari, A.P. Rendell, J.C. Burant, S.S. Iyengar, J. Tomasi, M. Cossi, J.M. Millam, M. Klene, C. Adamo, R. Cammi, J.W. Ochterski, R.L. Martin, K. Morokuma, O. Farkas, J.B. Foresman, D.J. Fox, "Gaussian 16 Rev. B.01," ed. Wallingford, CT, 2016.
[55] E. Ruiz, J. Cano, S. Alvarez, P. Alemany, Broken symmetry approach to calculation of exchange coupling constants for homobinuclear and heterobinuclear transition metal complexes, J. Comput. Chem. 20 (13) (1999) 1391–1400.
[56] E. Ruiz, A. Rodríguez-Fortea, P. Alemany, S. Alvarez, Density functional study of the exchange coupling in distorted cubane complexes containing the Cu_4O_4 core, Polyhedron 20 (11-14) (2001) 1323–1327.
[57] L. Noodleman, E.R. Davidson, Ligand spin polarization and antiferromagnetic coupling in transition metal dimers, Chem. Phys. 109 (1) (1986) 131–143.
[58] R. Boča, Zero-field splitting in metal complexes, Coord. Chem. Rev. 248 (9-10) (2004) 757–815.
[59] G. Christou, D. Gatteschi, D.N. Hendrickson, R. Sessoli, Single-molecule magnets, MRS Bull. 25 (11) (2000) 66–71.
[60] A.-L. Barra, L.-C. Brunel, D. Gatteschi, L. Pardi, R. Sessoli, High-frequency EPR spectroscopy of large metal ion clusters: from zero field splitting to quantum tunneling of the magnetization, Acc. Chem. Res. 31 (1998) 460–466.
[61] J. Krzystek, S.A. Zvyagin, A. Ozarowski, A.T. Fiedler, T.C. Brunold, J. Telser, Definitive spectroscopic determination of zero-field splitting in high-spin cobalt (II), J. Am. Chem. Soc. 126 (7) (2004) 2148–2155.
[62] T.A. Bazhenova, L.V. Zorina, S.V. Simonoy, V.S. Mironov, O.V. Maximova, L. Spillecke, C. Koo, R. Klingeler, Y.V. Manakin, A.N. Vasiliev, E.B. Yagubskii, The

first pentagonal-bipyramidal vanadium (III) complexes with a Schiff-base N_3O_2 pentadentate ligand: synthesis, structure and magnetic properties, Dalton Trans. 49 (2020) 15287–15298.
[63] N.I. Neuman, E. Winkler, O. Peña, M.C.G. Passeggi, A.C. Rizzi, C.D. Brondino, Magnetic properties of weakly exchange-coupled high spin Co(II) ions in pseudooctahedral coordination evaluated by single crystal X-Band EPR spectroscopy and magnetic measurements, Inorg. Chem. 53 (5) (2014) 2535–2544.
[64] Y. Oshima, H. Nojiri, K. Asakura, T. Sakai, M. Yamashita, H. Miyasaka, Collective magnetic excitation in a single-chain magnet by electron spin resonance measurements, Phys. Rev. B 73 (21) (2006), https://doi.org/10.1103/PhysRevB.73.214435.
[65] M. Rams, M. Böhme, V. Kataev, Y. Krupskaya, B. Büchner, W. Plass, T. Neumann, Z. Tomkowicz, C. Näther, Static and dynamic magnetic properties of the ferromagnetic coordination polymer $[Co(NCS)_2(py)_2]_n$, Phys. Chem. Chem. Phys. 19 (36) (2017) 24534–24544.
[66] Crystal Explorer 17, University of Western Australia. http://crystalexplorer.scb.uwa.edu.au/.
[67] P.R. Spackman, M.J. Turner, J.J. McKinnon, S.K. Wolff, D.J. Grimwood, D. Jayatilaka, M.A. Spackman, CrystalExplorer: a program for Hirshfeld surface analysis, visualization and quantitative analysis of molecular crystals, J. Appl. Crystallogr. 54 (2021) 1006–1011.
[68] K.S. Wolff, J.D. Grimwood, J.J. McKinnon, J.M. Turner, D. Jayatilaka, M.A. Spackman. CrystalExplorer (Version 3.1), University of Australia, 2012.
[69] J. Cano, E. Ruiz, S. Alvarez, M. Verdaguer, Spin density distribution in transition metal complexes: some thoughts and hints, Comment. Inorg. Chem. 20 (1998) 27–56.
[70] C. Desplanches, E. Ruiz, A. Rodríguez-Fortea, S. Alvarez, Exchange coupling of transition-metal ions through hydrogen bonding: a theoretical investigation, J. Am. Chem. Soc. 124 (2002) 5197–5205.